RSC Advances

ROYAL SOCIETY OF CHEMISTRY

PAPER

View Article Online
View Journal | View Issue

Cite this: *RSC Adv.*, 2023, **13**, 25846

A novel inclusion complex of oxybenzone with *C*-methylresorcin[4]arene deters skin permeation†

Xu Kang,[a] Andrew Eisenhart,[b] Ajaz Ahmad Dar,[a] Ramana Reddy Mittapalli,[a] Alexander Greenwood,[b] Lama Alsheddi,[a] Thomas L. Beck,[b] S. Kevin Li[a] and Harshita Kumari *[a]

Received 23rd March 2023
Accepted 17th August 2023

DOI: 10.1039/d3ra01890c

rsc.li/rsc-advances

Oxybenzone (OXB), a very widely used sunscreen ingredient has the potential to block both UVA and UVB but can penetrate through skin. Studies have revealed its presence in the blood and urine of most humans, which may lead to long-term health effects. As the confined cavities of macrocycles can alter the physical and chemical properties of encapsulated guests, in this study, we investigated the formation of host–guest complexes between *C*-methylresorcin[4]arene and OXB. Combined experimental (NMR spectroscopy, UV/vis absorption, and fluorescence spectroscopy) and theoretical investigation confirmed the formation of a weak host–guest complex that had a 1 : 1 stoichiometry. Furthermore, skin permeation testing revealed that complexation by *C*-methylresorcin[4]arene significantly reduced the skin permeation of OXB which can potentially limit the harmful effects of this organic sunscreen.

Introduction

Chronic exposure to UV radiation can cause various skin problems including sunburn, aging, and even melanoma (skin cancer).[1] Mid-range ultraviolet light (UVB, 280–320 nm) has been found to cause direct DNA damage; however, wavelengths that are not directly absorbed by DNA (UVA, >320 nm) can also induce skin damage.[2] In particular, DNA damage can be induced by wavelengths from 312 nm (in the UVB region) up to 434 nm (in the near-visible region) *via* the production of cyclobutane pyrimidine dimers and other photoproducts, which are associated with mutagenesis and cancer. This damage is not caused by the direct absorption of light but by the activation of photosensitizers that can generate singlet oxygen species.[3] By absorbing or reflecting UV radiation, sunscreens can prevent oxidative damage to DNA, thus keeping our skin from aging and protecting us from skin cancer. However, the instability and skin permeation of sunscreen ingredients remain concerning to both the industry and consumers. Oxybenzone (OXB) is a commonly used ingredient in sunscreens (Fig. 1a) that provides effective broad-spectrum ultraviolet coverage. However, beginning January 1, 2021, Hawaii has banned OXB-containing sunscreens to preserve coral reefs.[4] Moreover, OXB may have keratinocyte toxicity,[5] interrupt human hormones, and penetrate skin to enter the blood circulation system.[6] OXB can also permeate through the blood–brain barrier (BBB) and may significantly affect the neural development of children.[7] Unfortunately, OXB can be found in human breast milk,[8] thus endangering children's health. *In vivo* studies using the Franz diffusion cell have shown that 10% of OXB can penetrate human skin, with 0.4% entering the bloodstream and being eliminated through urine.[9,10] This result indicates that OXB can form complexes with substances in the adult human body to improve its water solubility, thus allowing urine excretion; however, little is known about the efficiency of this process in children.[9] A direct association has recently been found between OXB and Hirschsprung's disease (a neonatal intestinal abnormality derived from the failed migration of enteric neural crest cells) in infants under normal use conditions of sunscreen products by expecting mothers.[11] Although OXB permeation is not known to present any acute danger to adults, chronic effects and pediatric toxicities are still not fully understood. Furthermore, although OXB has recently been

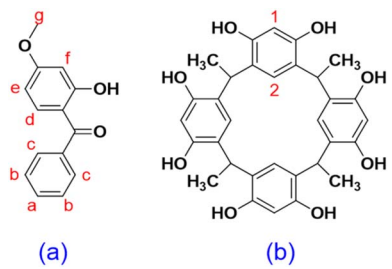

Fig. 1 Chemical structure of (a) oxybenzone; (b) *C*-methylresorcin[4]arene.

[a]*James L. Winkle College of Pharmacy, University of Cincinnati, 231 Albert Sabin Way, MSB 3109 C, Cincinnati, OH, USA. E-mail: kumariha@ucmail.uc.edu*

[b]*Department of Chemistry, College of Arts and Science, University of Cincinnati, 155 B McMicken Hall, Cincinnati, OH, 45221, USA*

† Electronic supplementary information (ESI) available. See DOI: https://doi.org/10.1039/d3ra01890c

shown to be relatively stable as compared to avobenzone (AVOB) and ecamsule (ECAM),[12] it can be easily oxidized under natural sunlight. As the oxidation of OXB can inactivate antioxidant systems,[13] OXB as a sunscreen ingredient is a potential source of skin irritation. Thus, both the instability and skin permeability of OXB are growing concerns.

Various attempts have been made in recent years to reduce the side effects of OXB. Cross *et al.* proposed increasing the viscosity of sunscreen formulations to reduce skin permeation by OXB. Although large amounts of a thickening agent were found to decrease skin permeation, this effect was offset when the solution was applied as a thin layer.[14] Felton *et al.* used hydroxypropyl-β-cyclodextrin to decrease OXB skin permeation and accumulation. Increases in permeation and accumulation were observed with 10% (w/w) hydroxypropyl-β-cyclodextrin, whereas both decreased with 20% (w/w) hydroxypropyl-β-cyclodextrin. This data indicated the potential formation of a drug reservoir on the skin, but complex formation was not verified using NMR or other analytical techniques.[15] Moreover, no studies have explicitly focused on using macrocycles to modify OXB and potentially address drug safety issues.

The confined space of a host molecule can provide both a boundary and free space within the cavity for a guest. A host can also provide conformation selectivity, depending on the free space available, the flexibility of the host, and the interactions between the host and the guest. Previous studies have shown that the hydrophobic cavities of many macrocycles can fine-tune the chemical properties of guests by, for example, improving solubility and stability, providing product selectivity, and changing fluorescence properties. Therefore, in this study, the effect of host–guest complexation with *C*-methylresorcin[4]arene (RsC1) (Fig. 1b), a macrocyclic host, on the chemical properties of OXB (Fig. 1a) was investigated. In particular, complex formation was examined using NMR spectroscopy, UV/vis absorption and fluorescence spectroscopy, the inclusion geometry was elucidated using molecular dynamics docking simulations, and the effects of host–guest complexation on skin permeation were determined using the Franz diffusion cell.

Experimental

Materials and methods

OXB was purchased from Sigma-Aldrich. RsC1 was synthesized using a solvent-free protocol as described by Tunstad *et al.*[16] and Elidrisi *et al.*[17] Phosphate-buffered saline (PBS) tablets (pH 7.4) were purchased from MP Biomedicals (Solon, OH). Sodium azide was purchased from Acros Organics (Morris Plains, NJ). Deuterated solvents were purchased from Sigma-Aldrich and Cambridge Isotope Laboratories. Split-thickness human cadaver skin (from males and females between the ages of 45 and 70 years) was obtained from the New York Firefighters Skin Bank (New York, NY). TEWL was measured using Delfin vapometer (Kuopio, Finland). NMR spectra were obtained using an AV 400 MHz NMR spectrometer (Bruker AV-400, Coventry, UK).

NMR titration. All ^{1}H-NMR spectra were obtained using a 400 MHz NMR AVANCE spectrometer (Bruker AV-400, Coventry, UK). Stock solutions (0.026 mM) of OXB and RsC1 were prepared using ethanol-d_1. In different NMR tubes, the host (RsC1) was gradually added to the guest (OXB) at molar ratios from 0 : 1 to 8 : 1, ensuring that each tube contained the same amount of deuterated solvent (0.8 ml). The tubes were sonicated and shaken vigorously until the solutions were well mixed, and then NMR spectra were recorded.

DOSY and NOESY. Very concentrated OXB (60 mg ml^{-1}) and OXB + RsC1 (60 mg ml^{-1} + 143 mg ml^{-1}) solutions were prepared in ethanol-d_1 and ethanol-d_6. The host (RsC1) was added to the guest (OXB) at a molar ratio of 1 : 1. The tubes were sonicated and shaken vigorously until the solutions were well mixed, and then DOSY and NOESY spectra were collected.

Absorption and fluorescence spectra measurements

Absorption spectra were measured using a SpectraMax Plus 384 spectrophotometer. Absorbance spectra were measured from 220 to 600 nm. All solutions were measured in 1 cm^2 quartz cuvettes with Teflon stoppers. Fluorescence spectra were recorded on a Varian Cary Eclipse Fluorescence spectrophotometer, in 3 ml quartz cuvettes operating at room temperature. The excitation wavelength was 290 nm, and emissions were recorded from 280 nm to 550 nm, using slit widths of 2.5 nm. Fluorescence titrations were performed in ethanol, and stock solutions of the host and guest were prepared with a concentration of 10 mM. Freshly prepared working solutions were made by diluting the stock solution to the required concentration.

Docking. Host–guest docking was explored using classical molecular dynamics simulations. Systems with host/guest ratios of 1 : 1, 2 : 1, and 4 : 1 were simulated over long timescales to sample the docking interactions. The molecular dynamics simulations were conducted using the Gromacs-2019.2 [18,19] suite of programs, utilizing the CHARMM general force field to represent the host and guest molecules.[20,21] The presented results were sampled from production simulations of 200 ns, which were preceded by system equilibration using the Nose–Hoover thermostat (0.1 ps coupling time) and the Parrinello–Rahman barostat (1.0 ps coupling time).[22,23] Spatial distribution functions were calculated using the trajectory analyzer and visualizer (TRAVIS).[24]

Skin preparation. Skin permeation studies of OXB were performed using split-thickness human skin in a Franz diffusion cell with a 0.7 cm^2 diffusion area. The same group of 3–4 skin donors was used in each experiment. The skin ID are CC031215, RT122315, SL041415, SW0472515. The use of human tissues was reviewed by the Institutional Review Board (IRB) at the University of Cincinnati (IRB #2013-8030) and #05-10-2; exemption under CFR (b) paragraph. To prepare the skin samples, the cadaver skin was cut into 1.5 cm × 1.5 cm pieces, thawed in Petri dishes with PBS at room temperature for 2 h, and then patted dry with Kimwipes before being mounted onto the diffusion cell with the stratum corneum side facing up. PBS containing 0.02% sodium azide as a preservative and 3% cyclodextrin as a solubilizing agent for OXB was used as the solution in the receptor chamber. The TEWL of the skin sample was measured to ensure skin integrity before the permeation

study. For TEWL measurements, a vapometer was placed on top of the donor chamber of the diffusion cell and the measurement was repeated until a constant TEWL value was obtained (2–3 measurements, 15 min apart). Only skin samples with TEWL values of <10 g m^{-2} h^{-1} were used for permeation experiments.

Permeation study. After the TEWL measurement, the skin in the diffusion cell was allowed to equilibrate for 1 h. During this equilibration period, the skin surface was maintained at 32 ± 1 °C. The receptor medium was stirred with a magnetic stirrer at 600 rpm to ensure uniform mixing. The permeation study was initiated by applying 2 mg cm^{-2} of the test formulation on the skin surface in the diffusion cell. The dose of 2 mg cm^{-2} was selected based on FDA guidelines. The test formulations were 6% OXB and 6% OXB + RsC1 (1 : 1) in ethanol. At 0, 3, 6, 10, 12, and 24 h after dosing, 0.5 ml samples were withdrawn from the receptor chamber and immediately replaced with the same volume of fresh PBS solution to maintain a constant receptor solution volume. At the end of the experiment, the residual formulation in the donor compartment was recovered by rinsing once with the receptor chamber solution (PBS with 0.02% sodium azide and 3% cyclodextrin) and four times with methanol/water (85 : 15) solution (each time with 0.5 ml for 30 s). The treated areas were then dried with Kimwipes. The donor chamber cap and gasket were soaked in 5 ml of methanol/water (85 : 15) solution for 30 min. The skin was then removed from the diffusion cell, cut into small pieces, and extracted with 4 × 1 ml of methanol/water (85 : 15) solution. Blank skin samples were used as the control. The samples collected from the receptor chamber, the rinses, and skin extraction were centrifuged (3000×*g* for 15 min), and OXB content in the supernatant was determined using HPLC. Statistical analysis was performed using the Student's unpaired *t*-test and $p < 0.05$ was considered significant.

HPLC. The HPLC assay was conducted using a Shimadzu HPLC system (Shimadzu Scientific Instruments, Inc., Addison, IL) with an LC-20 AT pump, an SPD-20A UV-vis detector, a SIL-20A autoinjector, and a Microsorb-MV100-5 C18 column (150 × 4.6 mm, Agilent Technologies, Santa Clara, CA). The mobile phase was methanol and water at a ratio of 85 : 15. The flow rate was 0.8 ml min^{-1}. The detection wavelength for OXB was 294 nm (absorption maximum of OXB) and the detection limit was 10 ng ml^{-1}. A calibration curve was constructed using OXB standards at concentrations between 10 ng ml^{-1} and 120 μg ml^{-1} and linearity was observed in this range. The concentration of OXB in the samples was calculated based on the calibration curve. To examine whether the recovery was related to the extraction method using the mobile phase, a control recovery study was performed in which skin in a vial was dosed with OXB with and without RsC1. The recovery of OXB was 83.6% and that of OXB + RsC1 was 137.4%. In the latter case, the recovery was higher than 100% due to RsC1 interference in the OXB assay, as RsC1 also absorbed at 294 nm and had a similar retention time in the HPLC chromatogram (Fig. S9, and S10†). Therefore, the experimental recovery of OXB in the permeation study was corrected using this information. To determine the concentration of RsC1 and confirm the absence of RsC1 interference in the OXB assay for the receptor chamber samples, calibration curves were constructed at 285 and 325 nm for both OXB and RsC1 using standards of 0–12.5 μg ml^{-1}. The calibration curves showed linearity in this concentration range, with RsC1 contributing to the absorbance at 285 nm but that at 325 nm being predominantly due to OXB (AUC *vs.* concentration slopes of 1.2 × 10^6 and 5.4 × 10^5 for OXB and RsC1, respectively, at 285 nm, and 8.3 × 10^5 and 2.8 × 10^2 for OXB and RsC1, respectively, at 325 nm). The concentration of RsC1 in the receptor chamber at 24 h was calculated from comparing the concentration difference between the concentration of OXB at 325 nm (at this wavelength the absorption of RsC1 was negligible) and the concentration of OXB at 285 nm (at this wavelength both OXB and RsC1 had absorption).

Results and discussion

^{1}H NMR titrations

Host–guest complexation between RsC1 and OXB was investigated using ^{1}H NMR spectroscopy. Fig. 2 shows the ^{1}H NMR spectra of OXB with increasing concentrations of RsC1. As RsC1 was added, the aromatic peaks at 7.4–7.7 ppm shifted upfield, indicating the formation of a complex between the RsC1 and OXB. The peaks continued to move up to an OXB/RsC1 ratio of 1 : 8, however, indicating that under these conditions the OXB–RsC1 interaction was weak to achieve complete saturation. Complexation between OXB and RsC1 was further investigated using 2D ^{1}H diffusion-ordered spectroscopy (DOSY).

DOSY analysis

The DOSY spectra of OXB, RsC1, and the OXB + RsC1 complex are shown in Fig. S1.† The DOSY spectra of pure OXB and RsC1 gave diffusion rates of approximately 10^{-9} and $10^{-9.4}$ m^2 s^{-1}, respectively (Fig. S1a and S1b†). In contrast, the DOSY spectrum of the OXB + RsC1 mixture (60 mg ml^{-1} + 143 mg ml^{-1}) gave slower diffusion rates of $10^{-9.4}$ and $10^{-9.7}$ m^2 s^{-1} corresponding to OXB and RsC1, respectively (Fig. S1c†). This can be taken as evidence of binding, but not complete saturation of OXB by RsC1. In that case, the OXB peaks would be expected to correspond to a full-formed complex and yield an equivalent or slower diffusion rate than the RsC1 peaks. Since this was not the

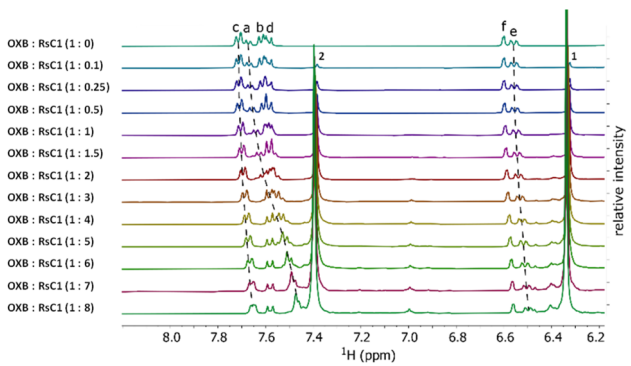

Fig. 2 ^{1}H NMR titration of OXB with RsC1 in ethanol-d_1.

case, it can be concluded that under the investigated experimental conditions, the complex was not formed to completion. Or in other words occupancy of guest within host was not 100% of the time.

NOESY analysis

2D NOESY studies have often been applied for the analysis of inclusion complexes to provide detailed structural information. The NOESY spectra can provide the spatial interaction between the ^{1}H-nuclei of the host and guest molecules and those cross-peak intensities depend on internuclear distances of ^{1}H-nucleus. 2D NOESY spectrum (Fig. S2†) of 1 : 1 mixture displayed intermolecular cross-peaks between RsC1 and OXB. There are clear cross-peaks between –CH_3 protons of RsC1 and H_c protons of OXB, considering that phenyl ring of OXB is located at the cavity port of RsC1. However, very lower-intensity cross-peaks observed between H_a and H_b with Rs-CH_3 even the NOESY spectrum was a "good" spectrum with no obvious problems. Furthermore, we run the NOESY spectrum using different delay values of D1 and D8 other than default values, surprisingly the spectra was same.

These finding proves the successful preparation of the RsC1–OXB inclusion complexes. Based on ^{1}H NMR titrations, combined DOSY and NOESY studies, the possible inclusion confirmation of OXB–RsC1 complex, in which the benzene ring of OXB is associated with the upper rim of an RsC1 molecule, whereas the methyl group of OXB interacts with the lower rim of another RsC1 molecule (Fig. 3).

Photophysical studies

The UV-vis and fluorescence studies were carried out to further strengthen the complexation of the RsC1–OXB system. The equimolar solutions of the OXB (0.02 mM) and RsC1 (0.02 mM) were prepared and mixed to standard volumes and proportions in order that the total concentration remained constant. The resultant absorption maxima at any particular concentration of the OXB and RsC1 increases relatively. A clearly observed isosbestic point at ~242 nm (Fig. S3†) illustrated that a well-defined supramolecular complexation in the current host–guest binding system and also suggests a 1 : 1 complex.[25]

The fluorescence titration experiments of RsC1 (0.02 mM) were performed with increasing concentrations of OXB (0–4 equiv). The fluorescence intensity of the RsC1 were decreased abruptly with the addition of OXB until the maximum complexation equilibrium was reached at 0.02 mM OXB concentration. The fluorescence intensity started decreasing slowly with further addition of the OXB concentration. Thus, the optimal host–guest ratio was selected as 1 : 1 and the RsC1 and OXB concentrations were both 0.02 mM. Moreover, the fluorescent intensity of the resulting solution was almost quenched (~92%), when 4 equiv. of OXB were added to RsC1 solution (Fig. S4†). It seems that a concentration-dependent quenching of the fluorescence of RsC1 occurred. This suggests that there is a weak interaction between RsC1 and OXB. Interestingly, OXB itself did not exhibit any fluorescence intensity under the same experimental conditions. One possible explanation for this situation is that the skeleton of RsC1 provides an optimal platform for the OXB molecule. It could be that the rigidity or flexibility of the RsC1 skeleton, along with a suitable cavity diameter, creates an environment that enhances the interaction between RsC1 and OXB, leading to the observed fluorescence quenching. This suggests that the specific structural features of RsC1 are crucial for accommodating and interacting with the OXB molecule effectively.

Job's plot and binding constant for the RsC1–OXB complex. Job's plot[26] experiment was carried out to determine the stoichiometry of the complex formed between RsC1 and OXB. From the fluorescence titration data obtained by the continuous variation method under a constant total concentration and systematically varying molar fractions of the components. A maximum value for the RsC1–OXB complex appears at the molar fraction of ~0.5, indicating that 1 : 1 stoichiometric complexation (Fig. S5†).

The binding constant (K) for the neutral form of RsC1 with the OXB guest has been estimated considering the 1 : 1 stoichiometry. The emission spectra of a fixed concentration of RsC1 have been recorded for different concentrations of OXB. The changes in the emission intensity at 320 nm due to the addition of OXB have been analyzed by the following modified Benesi–Hildebrand equation for 1 : 1 complexation.[27]

$$\Delta F = F_0 + FK[\mathrm{OXB}]/1 + K[\mathrm{OXB}] \quad (1)$$

Where ΔF represents the changes in the emission intensity of RsC1 due to the addition of OXB. F_0 and F are the emission intensity of RsC1 when it is completely free and bound to OXB, respectively. The changes in the emission intensity have been fitted with eqn (1) and the fitted result is shown in Fig. S6.† Significantly high correlation (R^2 = 0.9967) between experimental and fitted data further supports the fact that 1 : 1 complexation takes place between RsC1 and OXB. The value of K thus estimated from the fitting is ~0.40 M^{-1}.

Stern–Volmer plot

Stern–Volmer analysis was used to examine the nature of the quenching process in the complexation of RsC1 and OXB.[28] Plotting relative emission intensities (F_0/F) against OXB concentration yields a linear plot as shown in Fig. S7.† As the complexation was already revealed, such a linear plot supports that the fluorescence quenching observed due to the interaction between the RsC1 and OXB follows static quenching

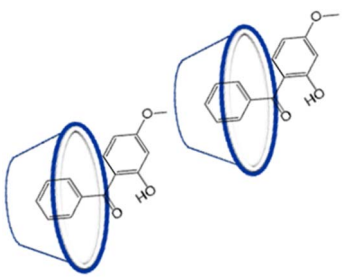

Fig. 3 Possible conformation of RsC1–OXB complex.

mechanism. The decrease in the emission intensity would be due to the formation of a supramolecular complex in the ground state of RsC1. The quenching constant value obtained is 0.072 M^{-1}. The slope of the line gives K_{sv}, the static quenching constant. F_0 and F are the initial and final fluorescence intensities respectively.

$$F_0/F = 1 + K_{sv}[\mathrm{OXB}] \quad (2)$$

Molecular dynamics docking simulations were used to gain insight into the inclusion geometry of the RsC1–OXB complex. OXB was predicted to primarily interact with the inner cavity of the host molecule, as indicated by the high-density areas in the calculated spatial distribution function of OXB (Fig. S8 top†).

The nature of the RsC1–OXB interaction was further characterized by monitoring the distance and angle between two encapsulating RsC1 molecules during interaction with an OXB molecule. The distance between two RsC1 molecules interacting through an OXB molecule was found to be centered at 10 Å (Fig. 4, left). In the distribution, two other peaks were observed (centered at 39 and 58 Å), corresponding to macrocycle pairs that had dissociated completely. Furthermore, the most favorable angle of interaction was found to be near 150°. These simulation results indicate that the partial encapsulation of an OXB molecule by two RsC1 molecules is possible.

To quantify the free space available in the RsC1 molecule, we monitored the size of the openings at the top and bottom of the macrocycle during the simulations (Fig. 5). Using these measurements, we can estimate the size of molecules that can associate with and sit within RsC1. The bottom opening showed narrow fluctuations around 5 Å, whereas the top opening showed two ranges centered at 7.5 and 9.75 Å. The bimodal nature of this distribution suggests that when associated with OXB, the top of the macrocycle may stretch to accommodate the guest.

By tracking the association of RsC1 and OXB during the molecular dynamics simulations, we quantified the average number of hosts associated with a guest molecule (Fig. 6). These results are based on the population of RsC1 molecules observed near the OXB molecule within a preset cut-off radius (Fig. 6). Increasing the cut-off radius increases the probability of detecting RsC1 molecules that interact with the OXB

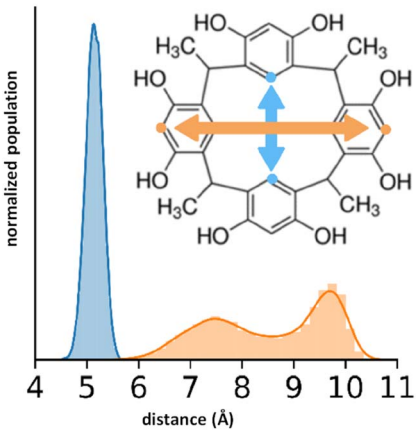

Fig. 5 Flexibility of the top (orange) and bottom (blue) openings of RsC1.

molecule; however, larger cut-off radii may also include RsC1 molecules that do not interact directly with the reference OXB molecule or it may include those that interact with the backside of another RsC1 molecule. Therefore, we determined the 8 (orange) and 10 Å (blue) cut-off radii to be the most relevant based upon the previously measured encapsulation distances between two RsC1 encapsulating an OXB. The most commonly observed association structure during the simulations involved a 1 : 1 interaction between RsC1 and OXB, which occurred approximately 20% and 33% of the time at 8 and 10 Å, respectively. In these cut-off ranges, 2 : 1 interactions between RsC1 and OXB were also observed, but the probability was nearly 10 times lower than that of the 1 : 1 interaction. No higher guest : host ratios were observed for the 2 and 5 Å cut-off radii. These simulation results show that although a 2 : 1 interaction is possible, but that the most common interaction between RsC1 and OXB is a 1 : 1 host–guest complex, with the OXB guest sitting deep inside the RsC1 host, which is in agreement with experimental findings. The interaction of two RsC1 with one OXB can also occur in this system, with the guest located between the two hosts.

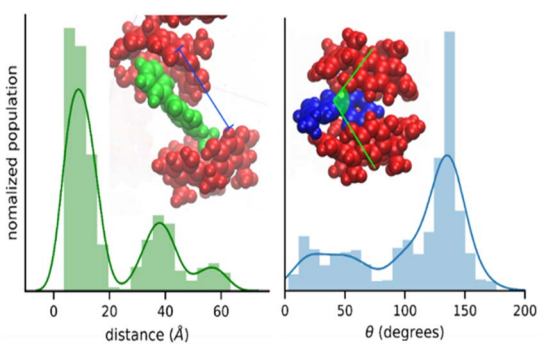

Fig. 4 Encapsulation geometry of RsC1–OXB defined by host–host distance (left) and host–guest–host angle (right).

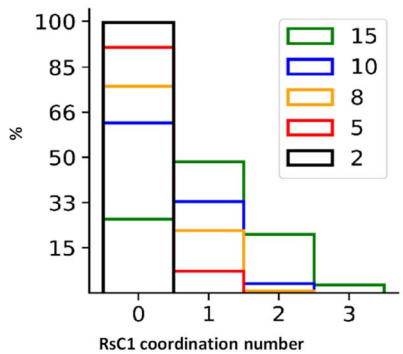

Fig. 6 Distributions of average number of RsC1 molecules associated with an OXB molecule at cut-off radii of 2, 5, 8, 10, and 15 Å.

The skin permeation of OXB was evaluated using 6% OXB formulations with and without RsC1 in a Franz diffusion cell (Fig. 7). In the OXB only group, 20.1% of the applied dose was found to penetrate the skin after 24 h. In the OXB + RsC1 group, skin permeation was significantly reduced and only 11.1% of the applied dose penetrated the skin (Student's unpaired *t*-test, $p = 0.016$). This result demonstrates that RsC1 complexation has an effect on OXB skin permeation. The amounts of OXB remaining on the skin surface, inside the skin, and on the surface of the donor chamber cap were also determined at the end of the skin permeation experiments. The average total recovery of OXB from the permeation study was approximately 75%. The recovery data indicate that a significant amount of OXB remained on the skin surface and that the amount of OXB remaining inside the skin was low when OXB was complexed with RsC1.

In addition, the amount of RsC1 that permeated through the skin to the receptor chamber was determined using an HPLC assay. As the amount of RsC1 permeated through the skin was found to be negligible (Fig. S11†), the skin permeation of RsC1 was insignificant under the conditions examined in this study. Together, these results suggest that RsC1 complexes OXB without permeating the skin, which could improve the safety of OXB-based sunscreen products.

(a)

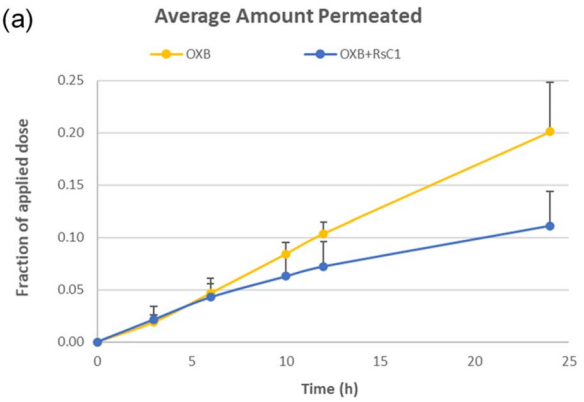

(b)

	OXB		OXB+RsC1	
	Average (%)	SD	Average (%)	SD
Receptor chamber	20.1	4.7	11.1	3.2
Rinse 1	24.0	7.5	5.8	0.6
Rinse 2	22.9	5.8	61.6	10.6
Skin cut-up	2.7	2.2	0.3	0.1
Donor chamber cap	0.6	0.4	0.9	0.2
Total OXB recovered	70.3	9.2	79.7	8.0

Fig. 7 (a) Skin permeation fractions of the OXB group (20.1% ± 4.7%; mean ± SD, $n = 3$) and the OXB + RsC1 group (11.1% ± 3.2%; mean ± SD, $n = 3$). (b) Recovery of OXB during skin permeation tests. Rinse 1: rinsing once using receptor chamber solution (PBS with 0.02% sodium azide and 3% cyclodextrin); rinse 2: rinsing four times using a methanol/water (85 : 15) solution. The values for the rinses, cut-up skin, and donor chamber cap were adjusted to correct for the extraction method and RsC1 interference during the OXB assay.

Conclusions

In this study, we investigated whether complexation by macrocycles could be used to prevent skin permeation by OXB, a common ingredient in sunscreens. Our results showed that OXB and RsC1 formed a 1 : 1 host–guest complex and that complexation dramatically decreased the skin permeation of OXB. Owing to the noncovalent interactions involved in host–guest complexation, this approach can be used to improve the chemical properties of the guest without altering its chemical composition. A more in-depth understanding of the effects of macrocycles on the chemical and pharmaceutical properties of photoactive compounds will provide novel methodologies for decreasing the instability, phototoxicity, and skin permeation of active ingredients, thus improving the overall safety of sunscreens and topical drugs.

Author contributions

XK: Data curation, formal analysis; AE: Data curation, formal analysis; AAD: Data curation, formal analysis; MRR: Data curation, formal analysis; AG: Methodology, software; LA: Data curation, formal analysis, methodology; TLB: Supervision, validation, writing-review and editing; SKL: Supervision, validation, writing-review and editing; HK: Conceptualization; resources; supervision, validation; writing-review and editing.

Conflicts of interest

There are no conflicts to declare.

Acknowledgements

This work was funded by UC Start-up funds (HK) and NSF-MRI grant CHE-1726092 and CHE-1955161 (TLB). The present address of TLB is the National Center for Computational Sciences, Oak Ridge National Laboratory, Oak Ridge, TN 37830.

Notes and references

1 Y. Matsumura and H. N. Ananthaswamy, Toxic effects of ultraviolet radiation on the skin, *Toxicol. Appl. Pharmacol.*, 2004, **195**, 298–308.
2 R. B. Setlow, E. Grist, K. Thompson and A. D. Woodhead, Wavelengths Effective in Induction of Malignant Melanoma, *Proc. Natl. Acad. Sci. U. S. A.*, 1993, **90**, 6666–6670.
3 E. Kvam and R. M. Tyrrell, Induction of oxidative DNA base damage in human skin cells by UV and near visible radiation, *Carcinogenesis*, 1997, **18**, 2379–2384.
4 R. B. Raffa, J. V. Jr Pergolizzi, R. Jr Taylor, J. M. Kitzen and N. R. Group, Sunscreen bans: Coral reefs and skin cancer, *J. Clin. Pharm. Ther.*, 2019, **44**, 134–139.
5 C. G. J. Hayden, S. E. Cross, C. Anderson, N. A. Saunders and M. S. Roberts, Sunscreen penetration of human skin and related keratinocyte toxicity after topical application, *Skin Pharmacol. Physiol.*, 2005, **18**, 170–174.

6 S. Kasichayanula, J. D. House, T. Wang and X. Gu, Percutaneous characterization of the insect repellent DEET and the sunscreen oxybenzone from topical skin application, *Toxicol. Appl. Pharmacol.*, 2007, **223**, 187–194.

7 A. Wnuk, J. Rzemieniec, J. Staroń, E. Litwa, W. Lasoń, A. Bojarski and M. Kajta, Prenatal Exposure to Benzophenone-3 Impairs Autophagy, Disrupts RXRs/PPARγ Signaling, and Alters Epigenetic and Post-Translational Statuses in Brain Neurons, *Mol. Neurobiol.*, 2019, **56**, 4820–4837.

8 D. Molins-Delgado, M. D. M. Olmo-Campos, G. Valeta-Juan, V. Pleguezuelos-Hernandez, D. Barcelo and M. S. Diaz-Cruz, Determination of UV filters in human breast milk using turbulent flow chromatography and babies' daily intake estimation, *Environ. Res.*, 2018, **161**, 532–539.

9 H. Gustavsson Gonzalez, A. Farbrot and O. Larkö, Percutaneous absorption of benzophenone-3, a common component of topical sunscreens, *Clin. Exp. Dermatol.*, 2002, **27**, 691–694.

10 R. Jiang, M. S. Roberts, D. M. Collins and H. A. E. Benson, Absorption of sunscreens across human skin: an evaluation of commercial products for children and adults, *Br. J. Clin. Pharmacol.*, 1999, **48**, 635–637.

11 J. C. Dinardo and C. A. Downs, Can Oxybenzone Cause Hirschsprung's Disease?, *Reprod. Toxicol.*, 2019, **86**, 98–100.

12 A. R. Abid, B. Marciniak, T. Pędziński and M. Shahid, Photo-stability and photo-sensitizing characterization of selected sunscreens' ingredients, *J. Photochem. Photobiol., A*, 2017, **332**, 241–250.

13 P. Kullavanijaya and H. W. Lim, Photoprotection, *J. Am. Acad. Dermatol.*, 2005, **52**, 937–958.

14 S. E. Cross, M. S. Roberts, R. Jiang and H. A. Benson, Can increasing the viscosity of formulations be used to reduce the human skin penetration of the sunscreen oxybenzone?, *J. Invest. Dermatol.*, 2001, **117**, 147–150.

15 L. A. Felton, C. J. Wiley and D. A. Godwin, Influence of hydroxypropyl-β-cyclodextrin on the transdermal permeation and skin accumulation of oxybenzone, *Drug Dev. Ind. Pharm.*, 2002, **28**, 1117–1124.

16 L. M. Tunstad, J. A. Tucker, E. Dalcanale, J. Weiser, J. A. Bryant, J. C. Sherman, R. C. Helgeson, C. B. Knobler and D. J. Cram, Host-guest complexation. 48. Octol building blocks for cavitands and carcerands, *J. Org. Chem.*, 1989, **54**, 1305–1312.

17 I. Elidrisi, S. Negin, P. V. Bhatt, T. Govender, H. G. Kruger, G. W. Gokel and G. E. M. Maguire, Pore formation in phospholipid bilayers by amphiphilic cavitands, *Org. Biomol. Chem.*, 2011, **9**, 4498–4506.

18 S. Pronk, S. Páll, R. Schulz, P. Larsson, P. Bjelkmar, R. Apostolov, M. R. Shirts, J. C. Smith, P. M. Kasson, D. van der Spoel, B. Hess and E. Lindahl, GROMACS 4.5: a high-throughput and highly parallel open source molecular simulation toolkit, *Bioinformatics*, 2013, **29**, 845–854.

19 S. Pall, M. J. Abraham, C. Kutzner, B. Hess and E. Lindahl, Tackling exascale software challenges in molecular dynamic simulations with GROMACS. Solving Software Challenges for Exascale. *International Conference on Exascale Applications and Software, EASC* 2014, *Stockholm, Sweden. Revised Selected Papers*, ed. S. Markidis and E. Laure, Springer Internat. Publ., Cham, 2015, pp. 3–27.

20 K. Vanommeslaeghe and A. D. MacKerell, Automation of the CHARMM General Force Field (CGenFF) I: bond perception and atom typing, *J. Chem. Inf. Model.*, 2012, **52**, 3144–3154.

21 K. Vanommeslaeghe, E. P. Raman and A. D. MacKerell, Automation of the CHARMM General Force Field (CGenFF) II: assignment of bonded parameters and partial atomic charges, *J. Chem. Inf. Model.*, 2012, **52**, 3155–3168.

22 S. Nosé, A unified formulation of the constant temperature molecular dynamics methods, *J. Chem. Phys.*, 1984, **81**, 511–519.

23 G. W. Hoover, Canonical dynamics: Equilibrium phase-space distributions, *Phys. Rev. A*, 1985, **31**, 1695.

24 M. Brehm, M. Thomas, S. Gehrke and B. Kirchner, TRAVIS – A Free Analyzer for Trajectories from Molecular Simulation, *J. Chem. Phys.*, 2020, **152**, 164105.

25 P. Thordarson, Determining association constants from titration experiments in supramolecular chemistry, *Chem. Soc. Rev.*, 2011, **40**, 1305–1323.

26 Z. Zhang, Y. Zou and C. Q. Deng, A novel and simple solvent-dependent fluorescent probe based on a click generated 8-aminoquinoline–steroid conjugate for multi-detection of Cu (ii), oxalate and pyrophosphate, *RSC Adv.*, 2017, **7**, 14742–14751.

27 H. A. Benesi and J. H. Hildebrand, A spectrophotometric investigation of the interaction of iodine with aromatic hydrocarbons, *J. Am. Chem. Soc.*, 1949, **71**, 2703–2707.

28 A. S. Jadhav, A. U. Chaudhari, K. M. Kodam and D. D. Malkhede, Photophysical and NMR studies of encapsulation of 2-cyano-6-hydroxy benzothiazole in p-sulfonatocalix [6] arene and its biological applications, *Analyst*, 2021, **146**, 5294–5306.